# Phase Change Cooling of Spacecraft Electronics: Terrestrial Reference Experiments Prior to ISS Microgravity Experiments

Karthekeyan Sridhar[1], Ryan Smith[1], Vinod Narayanan[2], Sushil Bhavnani[1]
[1]Department of Mechanical Engineering
Auburn University
Alabama 36849
Email: kzs0097@auburn.edu

[2] Department of Mechanical and Aerospace Engineering
2132 Bainer Hall
University of California Davis
Davis, CA 95616
Email: vnarayanan@ucdavis.edu

## ABSTRACT

This experimental, terrestrial study is part of a larger effort to dissipate increased heat fluxes through enhanced pool boiling in spacecraft electronics prior to an extensive study to be conducted on the International Space Station under pristine microgravity conditions. The absence of buoyancy forces in microgravity causes vapor bubbles to grow to a very large size, leading to premature critical heat flux (CHF). Using an engineered surface modification, namely an asymmetric sawtooth ratchet, to create mobility of the vapor mass can alleviate this problem. The stainless steel (SS 316L) test surfaces were fabricated using powder bed fusion, a metal additive manufacturing process. Vapor mobility was observed in the downward-facing configuration for the asymmetric sawtooth structure explored in the study. A thin liquid film was observed underneath the vapor bubbles as they slid along the microstructure. The asymmetric nature of this liquid film is explored using high-speed imaging at the crest and trough of the sawtooth. The proposed asymmetric saw-tooth microstructure is a potential technique to induce motion of vapor bubbles across electronic components when reduced buoyancy forces do not detach vapor bubbles from the surface.

**KEY WORDS:** two phase heat transfer, vapor mobility, microgravity, microstructured surface, passive pumping, electronics cooling

## NOMENCLATURE

| | |
|---|---|
| g | gravitational acceleration constant ($m/s^2$) |
| q” | heat flux ($W/cm^2$) |
| T | temperature (K) |
| P | pressure (atm) |

### Greek symbols

| | |
|---|---|
| µm | micrometer or micron ($10^{-6}$) |

### Subscripts

| | |
|---|---|
| w | wall |
| sat | saturation |

## INTRODUCTION

Microelectronic fabrication has moved towards smaller length-scales while also improving the error rates drastically with each leap in technology. This incredible advancement has also pushed auxiliary systems supporting this development towards improved predictive techniques. An important aspect of shrinking device form-factor is that heat fluxes, the heat dissipated from a unit area, has also risen. While previous generations of devices were maintained within operating limits using conventional cooling techniques like natural and forced convective cooling, next-gen devices require more aggressive techniques like phase-change cooling. Cooling solutions are further complicated in microgravity when buoyancy forces are negligible, as phase-change cooling methods depend on vapor mobility to provide high heat fluxes. This study is a preliminary step in a larger effort to induce vapor mobility in microgravity conditions without the aid of external devices such as pumps or complicated flow loops.

Surface profile modifications have been widely used in nucleate pool boiling to augment heat transfer using features like fins, grooves [1], reentrant cavities [2], [3] and other micro and nano structures[4]–[7]. A parallel branch of research based on the idea of creating pumpless loops through bubble-pumping has been explored through different devices such as hydrophobic membranes to collapse bubbles [8], tube with asymmetric cross-section to induce pressure differences [9] and vertical, parallel tubes to create density differences [10]. A particular variation of surface modification, namely an asymmetric sawtooth microstructure, has been shown to induce fluid motion while influencing heat transfer characteristics–essentially combining the two ideas represented above. Ratchet-like topography resembling the ones used in the current study has been explored by other researchers for different regions of the boiling curve. Linke et al. [11] reported pumping action caused due to asymmetric brass ratchets in the Leidenfrost regime for several fluids including R134a, ethanol and water. Apart from the net force induced by the microstructure, Linke theorized that thermocapillary flow along the ratchet’s length away from the wetting point might also be responsible for the net pumping of fluid along the horizontal direction. Dupeux et al. [12] investigated the dominant force inducing motion along the ratchets induced by the asymmetric flow assumed importance compared to inertial stresses for the

`

Leidenfrost regime. It is worth mentioning here that Stroock et al. [13] utilised the concept of asymmetric ratchets to create Marangoni-Benard convection in a thin layer of silicone oil to generate net flow.

Within the context of boiling heat transfer, Kapsenberg et al. [14] demonstrated fluid motion parallel to the microstructure due to nucleation from re-entrant cavities in a pool of FC-72. They also developed a semi-empirical model based on force balance, which was validated by an experiment conducted with deionized water. Thiagarajan et al. [15] conducted microgravity experiments in a parabolic flight and observed vapor bubbles moving at speeds as high as 27.4 mm/s across the ratcheted microstructure under reduced gravity. It was also reported that the bubble diameters were six times larger compared to microgravity.

Such discrepancies in vapor bubble dynamics have been reported by other researchers in microgravity across different experimental methods. The methods of investigation vary across drop towers, parabolic flights and experiments aboard the International Space Station (ISS). Xue et al. [16] studied nucleate pool boiling of FC-72 on a smooth surface under microgravity utilizing the Beijing drop tower. Two different modes of bubble growth and departure were observed depending on low or high heat flux being applied. In the low heat flux region, the bubbles grew to a large diameter but stayed attached to the surface with little to no coalescence. As the heat flux increased, the bubble density as well as bubble diameters increased significantly. Smaller bubbles were "sucked" into larger bubbles as a result of capillary flow along the heater's surface. The coalescence of smaller bubbles subsequently leads to departure of the large one due to momentum resulting from the coalescing process. An important conclusion from the authors suggested that thermocapillary forces may be an important mechanism helping the bubbles stay attached to the heater surface, aside from the lack of buoyancy forces.

Raj et al. [17] conducted over 200 pool boiling experimental runs in microgravity aboard the ISS using the Boiling eXperiment Facility (BXF). Semi-transparent microheaters were used to enable camera view through the array and bellows were used to maintain the pressure in the chamber between 0.57 atm-2.67 atm. The wall superheat required for onset of nucleate boiling was found to decrease with increasing pressure, and were lower compared to 1-g values. At low subcoolings ($\Delta T_{sub}$=1°C), heat transfer attributed to boiling was negligible as the bubble grew to a large size and covered the entire heater with vapor. The authors differentiated boiling in earth gravity and microgravity by describing them as buoyancy dominated boiling and surface tension dominated boiling respectively. A modified gravity scaling parameter to predict heat flux in microgravity was discussed and verified from the obtained experimental data.

Warrier et al. [18] studied nucleate pool boiling using a polished aluminum disc with five cylindrical cavities with four cavities placed at the corners of a square and one in the middle. The apparatus, termed the Nucleate Pool Boiling eXperiment (NPBX), was housed alongside Raj et al.'s [17] setup in the Microgravity Science Glovebox (MSG) aboard the ISS. The fluid used was FC-72, with a similar test setup including bellows and a flow test loop. The study observed that at low wall superheats during the onset of nucleate boiling, nucleated bubbles merged together to form a large central bubble in the middle of the square. This central bubble stayed on the heater surface and grew to large diameters. These observations are consistent with the other microgravity studies reported above, where the consensus is that bubbles stayed on the surface and grew to very large diameters. This situation severely inhibits heat transfer from the surface since the large vapor bubble poorly dissipates heat.

The present study aims to solve the problem of stationary vapor bubbles preventing quenching liquid to rewet the surface by a novel microstructure constructed of asymmetric saw teeth with square-shaped nucleation cavities. The engineered cavities were located on the long slope of the ratchet to preferentially direct vapor. The difference in radius of curvature between the peak and valley of the asymmetric saw-tooth produces a pressure differential which acts in tandem with the imbalance to impart passive, lateral bubble motion. The resulting bubble motion is a prospective technique to slide vapor across electronic heat sources in microgravity, when the diminished buoyancy forces are ineffective at detaching vapor bubbles. Preliminary NASA Zero-G flight experiments have demonstrated the viability of the passive bubble motion concept, prior to an extensive study to be performed on the ISS under prolonged microgravity conditions. The objective of the terrestrial study is to explore the vapor bubble dynamics offered by the asymmetric sawtooth structure with differing sawtooth angles, upward and downward facing orientations as shown in Figure 1, and differing nucleating site densities. The study was conducted to verify preferential vapor bubble motion offered by the ratchets in an experimental setup created to mimic the proposed ISS experiments. Boiling curves, along with high-speed imagery, were obtained to improve the predictability, reliability and reproducibility of similar microstructures in electronic devices.

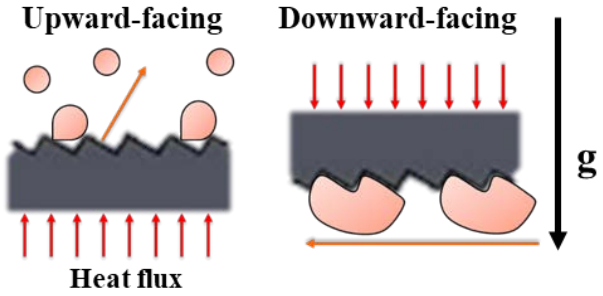


Figure 1 Schematic showing vapor mobility effected by the sawtooth microstructure in both upward-facing (left) and downward-facing (right) orientations.

## EXPERIMENTAL SETUP

The test surface consists of mirroring ratcheted sections separated by a central, unheated, flat section of 20 mm in length. The sawtooth structures have a pitch of 1 mm and consist of a 60°-30° structure, as shown in Figure 2. The dimensions of the test surface are 120 mm x 6 mm x 2mm (L x W x H). As shown in Figure 2, the test surface has a central, unheated, flat length of 20mm. The heated length of the ratchets

for the tests described in this study are 50 mm. The cavity density of the test surfaces varied as 1-mm or 2-mm apart. The test surfaces were fabricated using powder bed fusion, a metal additive manufacturing technique and were electropolished after heat treatment to obtain a smooth surface. The stainless steel surfaces used in this study were electropolished in-house to obtain a smooth surface and mirror finish. The electrolyte comprised of 25% wt. sulphuric acid and 75% wt. phosphoric acid while the cathode was a flat piece of stainless steel. The test surface to be polished was connected as the anode before being immersed into the solution.

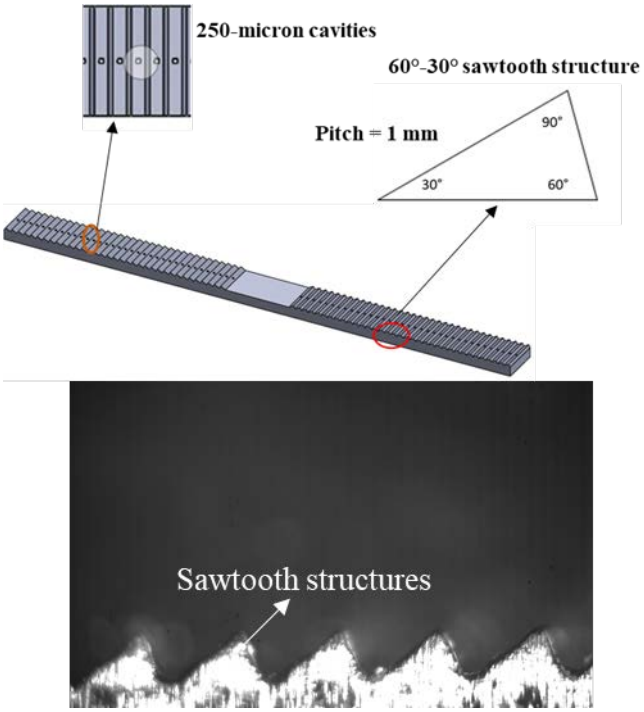


Figure 2 Details of additively manufactured test surfaces with differing sawtooth structures and 250 µm cavities (top). High-speed frame showing the microstructure in focus (bottom)

The Pore Formation and Mobility During Controlled Directional Solidification in a Microgravity Environment Investigation (PFMI) furnace available for ISS experiments (shown in Figure 3, top) currently can house a borosilicate glass ampoule with an outer diameter of 12 cm and a length of 30 cm to conduct experiments (shown in Figure 3, bottom). As this terrestrial experimental setup was created to closely align with the available dimensions of PFMI furnace, several features were fabricated using a combination of glass blowing techniques and metal-to-glass transitions. As the microstructure requires a flat surface, the 12 mm circular profile was converted into a square borosilicate glass tube with 8 mm I.D and 1.2 mm wall thickness with two square-circular transitions on either end for inlet and access ports. Two strategically located ports were added on the top face of the ampoule to facilitate positioning and adhering the specimen in the center of the glass tube. A T-shaped junction was created at the side face of the glass tube with two distinct pathways -the vertical path leads to the bellows where the effects of vapor expansion are mitigated, and the horizontal pathway leads to the data collection system. An end-located access port with a circular profile of 10 mm ID was used as a pathway for the k-type thermocouples. This design serves to mimic the final desired version of the ISS ampoule which will include circular transitions on both ends of the central square section to allow retrofitting into the PFMI furnace module on ISS. A stainless-steel bellows (2.375" (6.03 cm) I.D) with an empirically measured spring rate of ~26.97 N/mm was used to accommodate volume dilation due to vapor production during the experiment. The bellows is an aspect of the terrestrial experiment not expected to carry over to the ISS experiments. The complete experimental setup is shown in Figure 4.

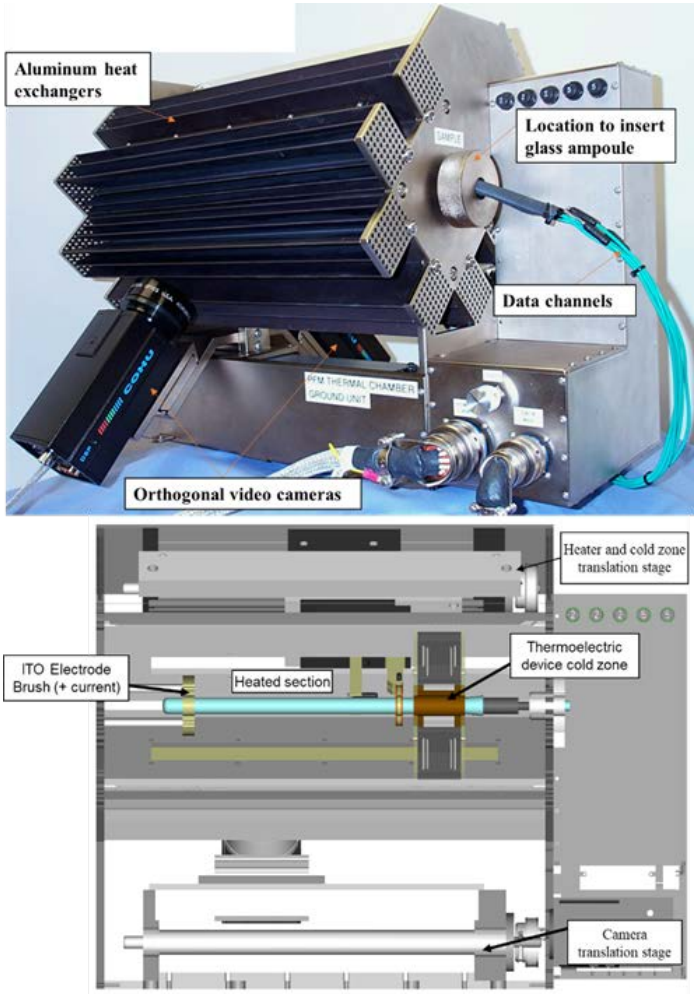


Figure 3 Feature of the PFMI furnace available for ISS experiments (top) and furnace section view (bottom)(adapted from [19])

The test surface was adhered to the glass using Arctic Silver thermal epoxy. Polyimide film heaters were mounted to the glass using Kapton™ adhesive and insulated using expanded polystyrene to ensure negligible heat loss. To mimic the thermoelectric device zone (TED) in the PFMI furnace

(shown in Figure 3, bottom), a few experimental runs were conducted using a regulated waterblock placed in the center of the borosilicate glass tube. However, test surface variations reported in the current study such as upward or downward-facing, sawtooth structure, nucleation site density were studied without use of the waterblock.

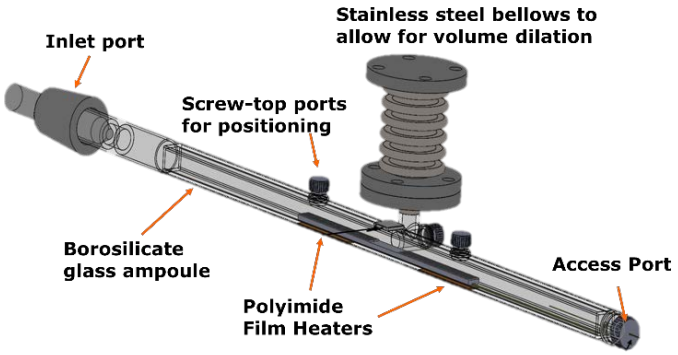


Figure 4 Isometric view of the complete ground experiment setup with positioning details of bellows and ports

A Phantom™ v310 high-speed camera outfitted with an Infinity microscope lens attachment was used to enable high-speed imaging. The dielectric liquid was degassed prior to experimental runs in the setup using a rope heater (Briskheat™ model HSTAT101006) wrapped around the bellows and a Graham condenser to ensure removal of non-condensable gases. A vacuum pump (Welch-Ilmvac™ Dryfast Ultra 2042) was connected to the inlet port and the dielectric liquid was charged using a modified flask to ensure minimal entrainment of non-condensables into the setup. Prior to a run, the tube was checked to be level for both orientations using a digital angle gauge calibrated to $\pm$ 0.1° by measurement at two locations on the horizontal, square section.

LabVIEW™ was used to measure all temperature data through interfacing with a data acquisition system. Two Omega™ K-type thermocouples were primarily used to measure temperature data at the surface, and the bulk liquid housed in the bellows. The thermocouples were calibrated against a NIST-traceable thermistor to provide a $\pm$0.2 K temperature data uncertainty. The pressure in the closed system was measured at the top of the bellows with a pressure transducer (Omegadyne™ model no. PX319-050A5V) capable of measuring up to 50 psi. The complete experimental setup was housed in a structure mounted on pneumatic vibration isolating feet (Newport™ SLM-1A) to reduce the effect of environmental noise such as equipment vibrations on vapor mobility dynamics.

## EXPERIMENTAL RESULTS AND DISCUSSION

The data reported in this section were collected in boiling experiments conducted using FC-72 with a subcooling of 20 K. The saturation temperature for each input heat flux was calculated based on the measured pressure of the closed system. The downward-facing configuration discussed in this study is the authors' attempt to bridge the terrestrial and microgravity experiments, by ensuring that vapor bubbles are not lifted off the surface due to buoyancy forces. The results of the test surfaces presented in this section were repeated at least twice for repeatability purposes. To reduce data redundancy and promote clarity of presented data, representative data is shown in each section below. A sample repeatability plot is shown in Figure 5.

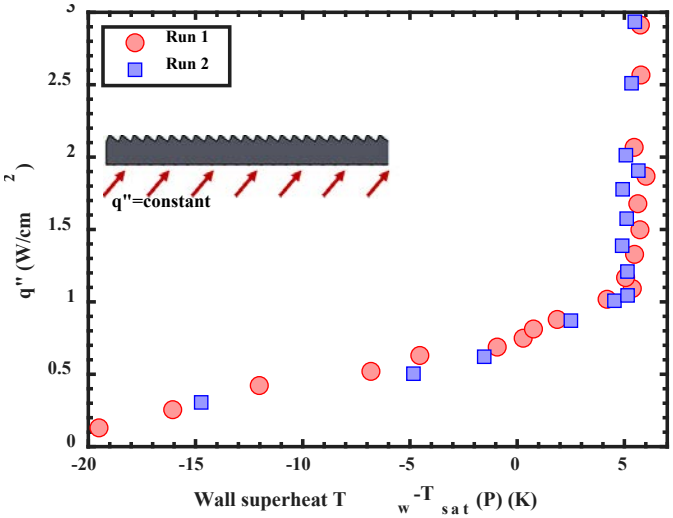


Figure 5 Repeatability plot for a 60°-30° sawtooth test surface with cavities spaced 1-mm apart

### Geometry effects

In a typical pool boiling scenario, a large "pool" of liquid is available to clearly distinguish the different boiling regimes and study the effects of a surface microstructure in detail. However, in the present study, the available liquid inventory within the tube is low enough to significantly alter boiling behavior – primarily due to vapor production. Combined with the fact that the microstructure induces flow in the downward facing configuration through vapor mobility, the lines between pool boiling and flow boiling are blurred. Due to the complex effects in play here, the results presented below cannot be interpreted within the limits of a conventional pool boiling setup.

As the heat flux nears the onset of nucleate boiling (ONB), the dielectric liquid (FC-72) starts creating vapor. Vapor starts travelling to the bellows to condense, and a liquid-vapor interface forms in the tube. With increasing heat flux, more vapor is created, eventually leading to dryout as shown in Figure 6. For the downward facing orientation, the effects of vapor production are more acute due to proximity to the liquid-vapor interface. Therefore, the dryout conditions for both orientations are not a limit of the liquid properties or microstructure but directly related to the low inventory afforded by the tube's confined cross section.

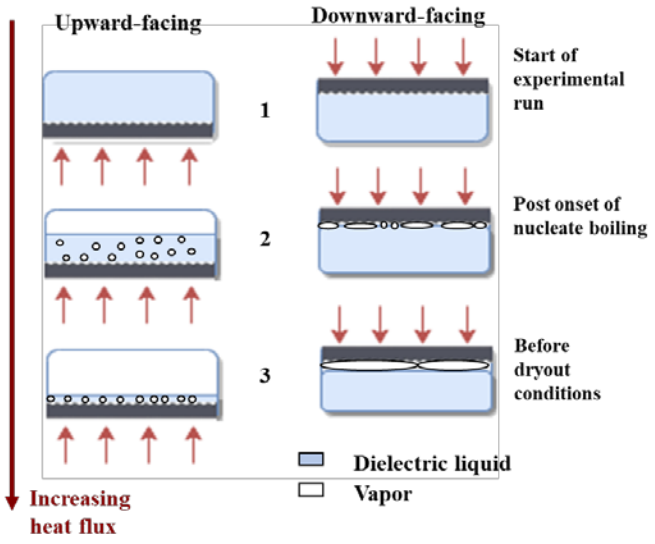


Figure 6 Schematic showing side-view of the cross-section of the square tube to demonstrate vapor production in the closed system at three stages during the experimental runs for both upward-facing and downward-facing orientations

**Effect of surface orientation (upward-facing vs downward-facing)**

As expected, the effect of surface orientation significantly altered boiling behavior as shown in Figure 7. For the downward-facing surface, nucleation is observed at heat fluxes as low as 0.88 W/cm$^2$ compared to 1.1 W/cm$^2$ for the upward facing surface. It is also seen that dryout is observed at 2.5 W/cm$^2$ for the downward facing surface, while similar dryout conditions were observed for the upward-facing orientation at ~3 W/cm$^2$. This limit is not attributed to the microstructure's efficacy in moving vapor but to the small, square cross section of the ampoule, which limits the amount of available liquid inventory. Though there is a clear pathway to the condenser (bellows) located centrally, vapor generation is high enough within the tube at higher heat fluxes to surpass outflow to the condenser. An interesting feature of the plot is the relatively low superheat required for onset of nucleate boiling (ONB) observed for the downward-facing surface.

**Upward-facing surfaces**

Bubble diameter and frequency was measured using frames extracted from the high-speed videos. The images were calibrated using known sawtooth dimension (1 mm pitch) and used to measure bubble departure diameter, departure frequency and velocity. The velocity of the departing bubbles was calculated using center of mass analysis, assuming that the vapor has uniform density throughout the bubble. Image J [20] was used for all image processing steps. At a heat flux of 1.05 W/cm$^2$ as described in Figure 8, the bubble departure diameter was consistently resolved between 1 and 1.12 mm with no significant decrease in diameter as the bubbles departed the surface within the frame of view. The departure frequency was observed to be between 38 and 41 Hz, with the velocity of departing bubbles maintained in the range of 71-77 mm/s. The vapor bubble's nucleation and growth along a 60°-30° sawtooth is illustrated in Figure 9.

To ensure that the lateral direction imparted to the vapor bubbles was not due to misalignment, the symmetric, mirrored ratcheted sections (as shown in Figure 2) were simultaneously heated. Alignment was confirmed as the vapor bubbles on the right half moved in opposite direction to the vapor bubbles on the left half, towards the tube's center.

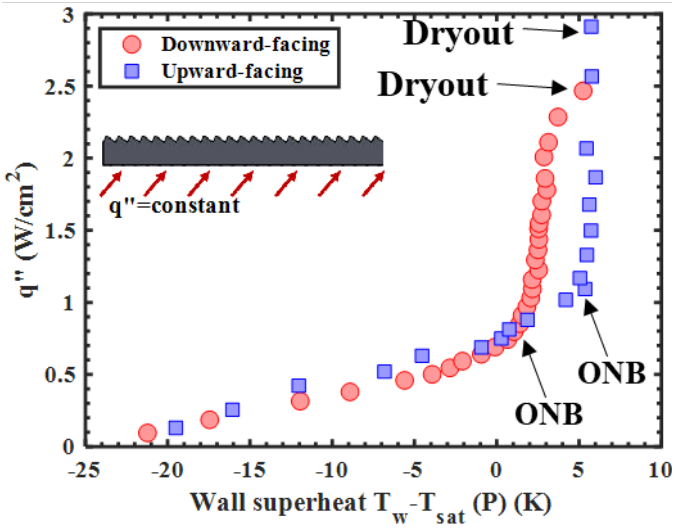


Figure 7 Wall superheat as a function of input heat flux for a 60°-30° sawtooth test surface with cavities spaced 1-mm apart

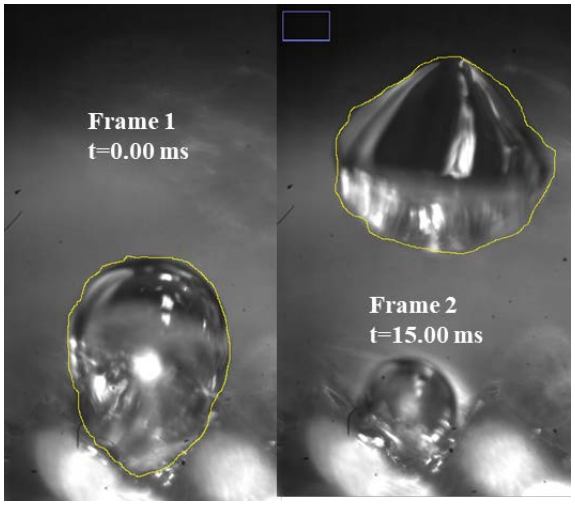


Figure 8 Sequence of images showing vapor bubble (outlined) nucleation and departure from a 250-micron cavity on 60°-30° sawtooth with the input heat flux at 1.05 W/cm$^2$. Due to the narrow depth of field afforded by the high-speed camera, the vapor bubbles are in sharp focus while the sawtooth features are blurred. (1280x800, 1000 fps)

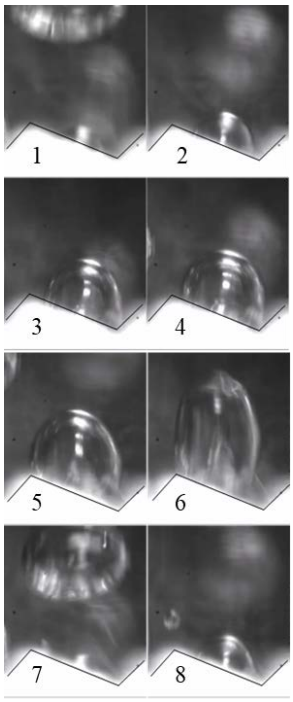


Figure 9 Series of images showing bubble nucleation and departure from a 250 µm cavity on a 60°-30° sawtooth (outlined in black) Frames 1-4 show the initial stages of bubble growth with a lateral component due to the surface microstructure. Frames 5-8 show the later stages of bubble growth and departure where the buoyancy forces dictate the departure direction. Bubble lifecycle was recorded over ~24 ms. (1280x800, 1000fps)

**Downward-facing surface**

For the downward facing surface, high-speed imaging was unclear with the 60°-30° sawtooth due to fluid perturbations. Therefore, a 75°-15° sawtooth structure was fabricated for better visualization of bubble dynamics. Flattened vapor bubbles were seen nucleating, coalescing and sliding across the surface from right to left in the nucleate boiling regime as shown in Figure 10. During nucleation incipience, multiple nucleated vapor bubbles were observed to coalesce before sliding along the microstructure. Sometimes, these coalesced bubbles would merge to form an even longer slug, which would quickly move across the microstructure in the intended (from right to left) direction. As the heat flux increased, the frequency of these slug formation events was observed to increase.

When the surface was covered by a fast-moving vapor slug, a subtle but distinct interface was seen moving along the asymmetric ratchets, as shown in Figure 11. Upon closer inspection, the liquid-vapor interface pattern was due to the vapor bubbles riding on a thin film of liquid, in line with observations by previous researchers who explored the dynamics of the asymmetric ratchet in microgravity[15]. When the Edge Sobel horizontal filter was applied to the image, the interface came into sharp focus. The liquid film was found to be asymmetric as the liquid film is thicker at the trough compared to the crest of the sawtooth. Current efforts are directed at studying the thickness of the liquid film for a variety of parametric conditions.

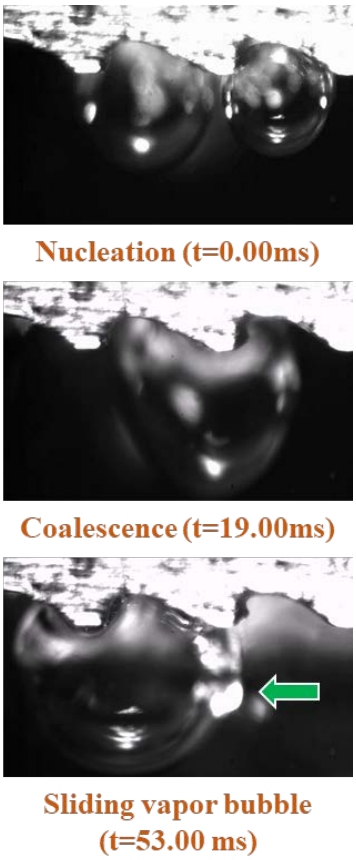


Figure 10 Sequence of images showing bubble nucleation, coalescence and sliding across the microstructure (from left to right) on a 75°-15° sawtooth in the downward-facing orientation (1280x800, 1000 fps)

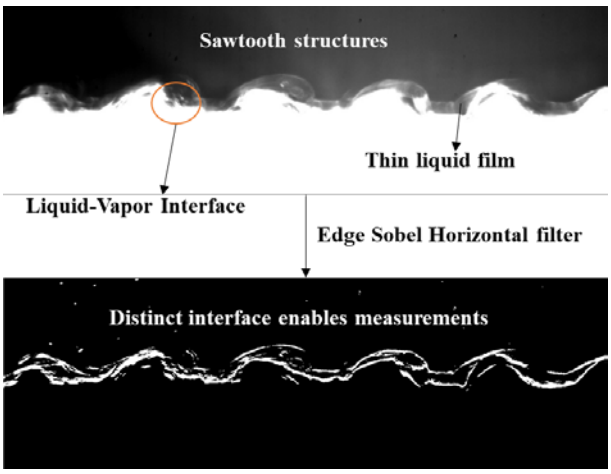


Figure 11 Liquid-vapor interface of a sliding vapor slug in FC-72 in a downward-facing orientation at 2.5 W/cm$^2$. When an edge filter is applied to the backlit, contrasted image, the interface comes into sharp focus to enable measurements. (1280x800, 700 fps)

**Cavity density for upward-facing surfaces**

For the test surfaces with cavities spaced 1-mm apart, the onset of nucleate boiling was observed at a superheat close to 4.5 K lower than the test surface with cavities spaced 2-mm apart, given a constant heating length as shown in Figure 12. This result is in line with expectations, and validates the role of 250 µm cavities as effective nucleation sites. Apart from significantly altering the boiling curves, the nucleation site density influenced the clarity of high-speed imaging. Vapor bubbles were easier to capture with high-speed imagery for test surfaces with cavities located 2-mm apart due to lower image distortion with the field of view as shown in Figure 13. For cavities located closer, the continuous nucleation and departure of vapor bubbles hindered clear imaging due to constant fluid motion.

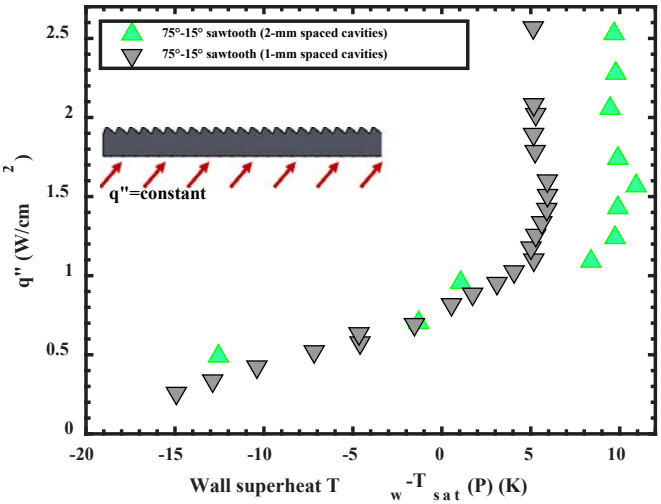


Figure 12 Effect of nucleation site density on upward-facing surfaces with a 75°-15° sawtooth structure

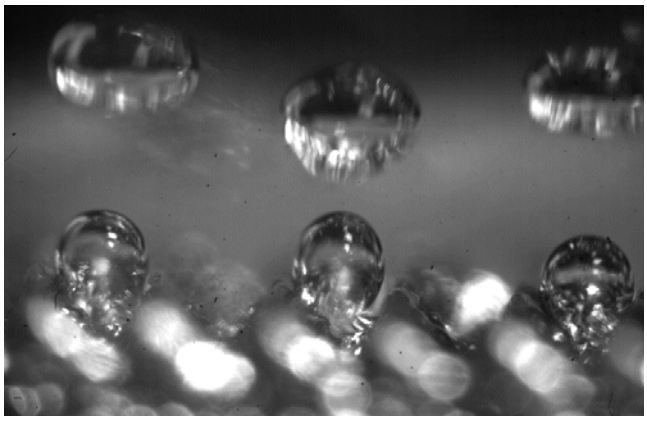

Figure 13 Bubble nucleation and departure from three 250-micron cavities on a 60°-30° sawtooth test surface with cavities spaced 2-mm apart. High-speed imaging is focused on the vapor bubbles due to low distortion from fluid motion. (1280x800, 1000fps)

Another important design consideration for the ISS experiments is the increase in system pressure during the experimental runs. Though vapor bubble dynamics are expected to be different in microgravity conditions, the terrestrial experiments provide a valuable frame of reference for design purposes. Across the variations of experimental runs performed in this study, the highest increase in pressure for the 50 mm test section was 0.216 atm.

## CONCLUSION

The borosilicate glass square tube with 8 mm I.D. resulted in the test surface trending towards dryout at heat fluxes as low as ~3 W/cm$^2$ for the upward-facing configuration and ~2.5 W/cm$^2$ for the downward-facing configuration. The downward-facing configuration is an attempt to mimic vapor mobility in microgravity conditions as buoyancy forces do not detach vapor bubbles from the surface. Vapor mobility actuated by the microstructure was observed for the downward-facing surface with distinct features such as nucleation, coalescence and subsequent sliding of the vapor bubbles. A thin liquid film was observed underneath coalesced bubbles and the thickness of the liquid film varied depending on the location at the sawtooth. The trough had a higher thickness than the crest for the conditions encountered in the study. The effect of nucleation site density was significant for the upward-facing configuration, resulting in a difference in superheat of 4.5 K during nucleation incipience. The discussed sawtooth microstructure is a feasible surface modification to passively enable phase-change cooling for spacecraft electronics.

## ACKNOWLEDGMENT

Financial assistance for the project was provided by NSF under grant number 1740515.

## REFERENCES

[1] T. M. Anderson and I. Mudawar, “Microelectronic Cooling by Enhanced Pool Boiling of a Dielectric Fluorocarbon Liquid,” 1989.

[2] K. G. Rajulu, R. Kumar, B. Mohanty, and H. K. Varma, “Enhancement of nucleate pool boiling heat transfer coefficient by reentrant cavity surfaces,” *Heat Mass Transf. und Stoffuebertragung*, vol. 41, no. 2, pp. 127–132, Dec. 2004.

[3] N. Nimkar, S. Bhavnani, R. J. of heat and mass Transfer, and U. 2006, “Effect of nucleation site spacing on the pool boiling characteristics of a structured surface,” *Elsevier*.

[4] S. Bhavnani *et al.*, “Boiling Augmentation with Micro/Nanostructured Surfaces: Current Status and Research Outlook,” *Nanoscale Microscale Thermophys. Eng.*, vol. 18, no. 3, pp. 197–222, Jul. 2014.

[5] L. Dong, X. Quan, and P. Cheng, “An experimental investigation of enhanced pool boiling heat transfer from surfaces with micro/nano-structures,” *Int. J.*

*Heat Mass Transf.*, vol. 71, pp. 189–196, Apr. 2014.
[6] X. Zheng and C. W. Park, "Experimental study of the sintered multi-walled carbon nanotube/copper microstructures for boiling heat transfer," *Appl. Therm. Eng.*, vol. 86, pp. 14–26, May 2015.
[7] K. H. Chu, R. Enright, and E. N. Wang, "Structured surfaces for enhanced pool boiling heat transfer," *Appl. Phys. Lett.*, vol. 100, no. 24, Jun. 2012.
[8] D. D. Meng and C. J. Kim, "Micropumping of liquid by directional growth and selective venting of gas bubbles," *Lab Chip*, 2008.
[9] X. Geng, H. Yuan, H. N. Oğuz, and A. Prosperetti, "Bubble-based micropump for electrically conducting liquids," *J. Micromechanics Microengineering*, 2001.
[10] S. Mukherjee and I. Mudawar, "Pumpless Loop for Narrow Channel and Micro-Channel Boiling," *J. Electron. Packag.*, 2003.
[11] H. Linke *et al.*, "Self-propelled leidenfrost droplets," *Phys. Rev. Lett.*, vol. 96, no. 15, 2006.
[12] G. Dupeux, M. Le Merrer, G. Lagubeau, C. Clanet, S. Hardt, and D. Quéré, "Viscous mechanism for Leidenfrost propulsion on a ratchet," *EPL*, 2011.
[13] A. D. Stroock, R. F. Ismagilov, H. A. Stone, and G. M. Whitesides, "Fluidic Ratchet Based on Marangoni-Bé nard Convection," 2003.
[14] F. Kapsenberg, L. Strid, N. Thiagarajan, V. Narayanan, and S. H. Bhavnani, "On the lateral fluid motion during pool boiling via preferentially located cavities," *Appl. Phys. Lett.*, 2014.
[15] N. Thiagarajan, … S. B.-J. of, and undefined 2015, "Self-Propelled Sliding Bubble Motion Induced by Surface Microstructure in Pool Boiling of a Dielectric Fluid Under Microgravity," *… .asmedigitalcollection.asme.org*.
[16] Y. F. Xue, J. F. Zhao, J. J. Wei, J. Li, D. Guo, and S. X. Wan, "Experimental study of nucleate pool boiling of FC-72 on smooth surface under microgravity," *Microgravity Sci. Technol.*, 2011.
[17] R. Raj, J. Kim, and J. McQuillen, "Pool Boiling Heat Transfer on the International Space Station: Experimental Results and Model Verification," *J. Heat Transfer*, 2012.
[18] G. R. Warrier, V. K. Dhir, and D. F. Chao, "Nucleate pool boiling eXperiment (NPBX) in microgravity: International space station," *Int. J. Heat Mass Transf.*, 2015.
[19] R. Spivey *et al.*, "AIAA 2003-1362 SUBSA and PFMI Transparent Furnace Systems Currently in use in the International Space Station Microgravity Science Glovebox SUBSA and PFMI Transparent Furnace Systems Currently in use in the International Space Station Microgravity Science Glovebox."
[20] C. A. Schneider, W. S. Rasband, and K. W. Eliceiri, "NIH Image to ImageJ: 25 years of image analysis," *Nature Methods*, vol. 9, no. 7. pp. 671–675, Jul-2012S.

`